Simultaneous functional and structural imaging for photovoltaic devices

Zibang Zhang[a,b,1], Manhong Yao[a,1], Xiang Li[a], Qiwen Deng[a], Qingyu Peng[c], Jingang Zhong[a,b,*]

[a] Department of Optoelectronic Engineering, Jinan University, Guangzhou 510632, China
[b] Guangdong Provincial Key Laboratory of Optical Fiber Sensing and Communications, Jinan University, Guangzhou 510632, China
[c] Department of Computer Science, Jinan University, Guangzhou 510632, China

ABSTRACT

The functionality of photovoltaic devices (such as, solar cells) is converting photons to electricity. Characterization of photovoltaic devices is essential at production level and during use. Here we put forward a new concept of functional imaging for photovoltaic devices. Based on the concept, we also propose an optical technique that can simultaneously acquire functionality and structure images of a single or multiple photovoltaic devices. The technique is simple, low-cost, effective, and efficient. It requires no mechanic motion and instead structured illumination is adopted for image acquisition. The complementary information provided by the functionality and structure images acquired allows one to better identify any existing and developing faults of photovoltaic devices. What's more, the technique is able to give reliable results with much fewer measurements than image pixels by exploiting the sparsity of functionality and structure images in the Fourier domain. The technique allows not only users to monitor the 'health condition' of the utilized devices, but also manufacturers to improve their fabrication conditions. The proposed technique may be applicable for rapid characterization for other semiconductor-based devices.

1. Introduction

Functional imaging is known as a medical imaging technique and aims at visualizing physiological activities within a certain tissue or organ to evaluate the risk or danger of developing some diseases, while structural imaging aims at visualizing and examining the structures of a tissue or organ so as to detect whether visible abnormalities exist. Thus, functional imaging and structural imaging [1–3] can jointly provide rich information about the health condition of a certain tissue or organ and underlying physiological process. Although functional imaging is a term that originates in the field of medical imaging, we consider that the concept of imaging the internal functionality of an object can be extended to many other fields. In this paper, we put forward the concept of functional imaging for assessing the 'health condition' of photovoltaic devices.

The basic functionality of photovoltaic devices is converting photons to electricity. Functional imaging of photovoltaic devices is referred to acquire a photocurrent quantum efficiency map of the devices while structural imaging of photovoltaic devices is referred to acquire the spatial reflectance/transmittance distribution of the devices. Functional and structural imaging of photovoltaic devices allows for fully characterizing the devices, e.g., validating its effectiveness,

detecting defects inside the devices, and achieving the current response map over the active area.

The photocurrent quantum efficiency mapping for two-dimensional (2-D) image sensors is also known as pixel response function measurement [4–9]. Typical current response mapping technique–laser beam-induced current (LBIC)–uses a motor driven and collimated laser spot to perform raster scan. High intensity of laser and precise mechanic motion enable high signal-to-noise and accurate response mapping. However, laser scanning approaches have difficulties in rapid response function measurement. It is because the acquisition of a complete functionality image of the target photovoltaic device requires that the whole active area of the device should be scanned throughout. Additionally, accurate measurement relies on precise mechanical motion which might be costly and time-consuming. Laser-scanning-based approaches might have also difficulties in measuring the response function for multiple devices simultaneously, because multiple motor driven scanning lasers are required and it adds expense and complexity. Modulation transfer function based approaches, which use laser interference to generate basis patterns, have been also reported [10–12]. However, interference requires crucial experimental conditions. Finely tuning the spatial frequency and the initial phase of the basis patterns is also tricky in practice. Recently, current response mapping of

---

photovoltaic devices by using digital micromirror device (DMD) [13–15] and compressive sensing [14,15] is reported. DMD is able to generate binary patterns at a high speed (over 20 kHz) and therefore can substantially accelerate LBIC measurements.

As functional information and structural information are complementary to each other, simultaneous functional and structural imaging for photovoltaic device can link functional features and structural features. Moreover, it can be done with a single experimental setup and needs not image registration. Simultaneous functional and structural imaging as a dual-modality imaging approach provides richer information than single-modality counterparts, allowing better photovoltaic devices characterization. However, simultaneous functional and structural imaging for photovoltaic device(s) has not been reported to our best knowledge, which drives us to explore this technique.

In this paper, we not only put forward a new concept of functional imaging for photovoltaic devices, but also propose a simultaneous functional and structural imaging technique for photovoltaic devices, termed 'func-structural imaging'. The technique employs a spatial light modulator to generate basis patterns for structured illumination. The technique is applicable for accurate photovoltaic response function measurement for a photovoltaic device. It can also potentially achieve rapid characterization for multiple photovoltaic devices. Moreover, the simultaneously derived functionality and structure images can be fused to provide rich information about the health condition of the devices. The fused image allows for an augmented ability to trace the defects or sensitivity abnormalities back to devices, assisting in diagnosis and further 'treatment'. More importantly, the functionality and the structure images can be reconstructed from a relatively small number of measurements (in comparison with the number of image pixels) for efficient measurement. With the multiple devices imaging ability, the technique is capable of performing rapid characterization for photovoltaic devices with a simple set-up. The technique may find potential applications in not only operational optimization and quality control during manufacture, but also semiconductors' defects identification.

2. Methods

Photovoltaic devices are semiconductor devices that convert light into an electrical current. The total generated current is dependent on the density of photons that strike the junction (namely, active area), the size of junction, and quantum efficiency of the junction (namely, sensitivity over the active area). The total current E through a photovoltaic device is the sum of the dark current (current that is generated in the absence of light) and the photocurrent. Here we propose to use time-varying structured patterns to illuminate the target photovoltaic device and measure the corresponding total current values, so as to acquire the functionality information of the device. As such, the functionality image can be recovered from the measured current values computationally.

As Fig. 1(a) shows, the functionality image is expressed in a discrete form $I_{\text{func}}(x, y)$ and we use a sequence of patterns, each of which is expressed as $P(x, y)$, to illuminate the photovoltaic device. When the device is under illumination by a single pattern, the resulting total output current, E, can be expressed as

$$E = \iint k\{I_{\text{func}}(x, y) \cdot [P(x, y) + P_0] \mathrm{d}x \mathrm{d}y\} + \varepsilon, \tag{1}$$

where (x, y) is a Cartesian coordinate of the device plane, $I_{\text{func}}(x, y)$ is the functionality image of a photovoltaic device with respect to coordinate x and y, $P(x, y)$ is an illumination pattern, P_0 is time-invariant ambient illumination, k is the photovoltaic conversion factor, and ε denotes a dark current. For the case of multiple photovoltaic devices, the devices are arranged as an array and configured in parallel, as Fig. 1(b) shows. In this case, every single illumination pattern covers all the photovoltaic devices and E in Eq. (1) denotes the sum of the output current of all devices.

Eq. (1) implies that the measurement E is an inner product of the illumination pattern and the functionality image. Our goal is to encode the 2-D spatial information of the functionality image into a 1-D sequence of output electric signals. Inspired by basis-scan single-pixel imaging [16–26], we propose to use a complete set of pre-defined orthogonal patterns for illumination. As such, every single measurement is equivalent to a coefficient of a certain orthogonal transformation specified by the illumination patterns. For example, if 2-D Walsh-Hadamard patterns are used, the measurements will be mathematically equivalent to Hadamard coefficients. With the Hadamard coefficients, the 2-D Hadamard transform of the functionality image can be acquired. To recover the functionality image, one can arrange the measurements (that is, Hadamard coefficients) in a form of a 2-D Hadamard spectrum and apply a 2-D inversed Hadamard transform to the spectrum. As it has demonstrated that Fourier single-pixel imaging outperforms Hadamard single-pixel imaging in terms of efficiency [26], we propose to use sinusoidal (Fourier basis) patterns for imaging.

Each sinusoidal pattern $P_{\varphi}(f_x, f_y, x, y)$ is characterized by a spatial frequency pair (f_x, f_y) and an initial phase φ,

$$P_{\varphi}(f_x, f_y, x, y) = a + b \cdot \cos[2\pi(f_x x + f_y y) + \varphi]. \tag{2}$$

In order to eliminate ambient illumination and improve the signal-to-noise ratio, we propose to perform differential measurement by 4-step phase-shifting strategy. Each complex-valued Fourier coefficient is derived from 4 measurements by using the 4-step phase-shifting method [16]. Specifically, to derive the Fourier coefficient $\tilde{I}_{\text{func}}(f_x, f_y)$, a set of 4 sinusoidal patterns, as shown in Fig. 1(c), with the identical spatial frequency pair (f_x, f_y) but a different initial phase φ is used. The four initial phases are 0, $\pi/2$, π, and $3\pi/2$, respectively. Assuming the resulting photovoltaic responses by the target photovoltaic device are denoted by D_0, $D_{\pi/2}$, D_{π}, and $D_{3\pi/2}$, the Fourier coefficient $\tilde{I}_{\text{func}}(f_x, f_y)$ can be calculated by

$$\tilde{I}_{\text{func}}(f_x, f_y) = (D_{\pi} - D_0) + \mathrm{j}(D_{3\pi/2} - D_{\pi/2}), \tag{3}$$

where j denotes the imaginary unit. As any functionality image is real-number, its Fourier spectrum is conjugated symmetric. Therefore, we only need to acquire one half of the Fourier coefficients in the Fourier space. As a result, fully sampling a functionality image with the 4-step phase-shifting method takes $2N$ measurements, where N equals to the pixel count of the functionality image. The functionality image can be reconstructed by applying an inverse 2-D Fourier transform to the spectrum acquired, that is,

$$I_{\text{func}}(x, y) = F^{-1}\{\tilde{I}_{\text{func}}(f_x, f_y)\} = F^{-1}\{(D_{\pi} - D_0) + \mathrm{j}(D_{3\pi/2} - D_{\pi/2})\}, \tag{4}$$

where $F^{-1}\{\}$ denotes an inverse 2-D Fourier transform operator. Please note that 2-D Walsh-Hadamard patterns are also a candidate for illumination. Please also note that exploiting the sparsity of functionality images potentially enables rapid image acquisition. The sparsity is referred to that most of the energy of functionality images and structure images concentrate at the low-frequency region in the Fourier domain. Thus, one can only sample the low-frequency Fourier coefficients in the Fourier domain instead of the complete Fourier spectrum so as to reduce the number of measurements, which is detailed in [16]. As will be demonstrated in the next section, the functionality image and the structure image reconstructed from under-sampled data is informative enough for photovoltaic detectors characterization.

To simultaneously obtain the structure image of a photovoltaic device, we propose to use a photovoltaic detector (termed side detector) to collect the reflected light by the target photovoltaic device which is under structured illumination. The structure image refers to a reflectance image of the target photovoltaic device. The data acquisition and reconstruction of the structure image is exactly the same as that of the functionality image. Specifically, by substituting the responses of the target photovoltaic device by those of the side detector into Eq. (4), one can derive the structure image of the target photovoltaic device.
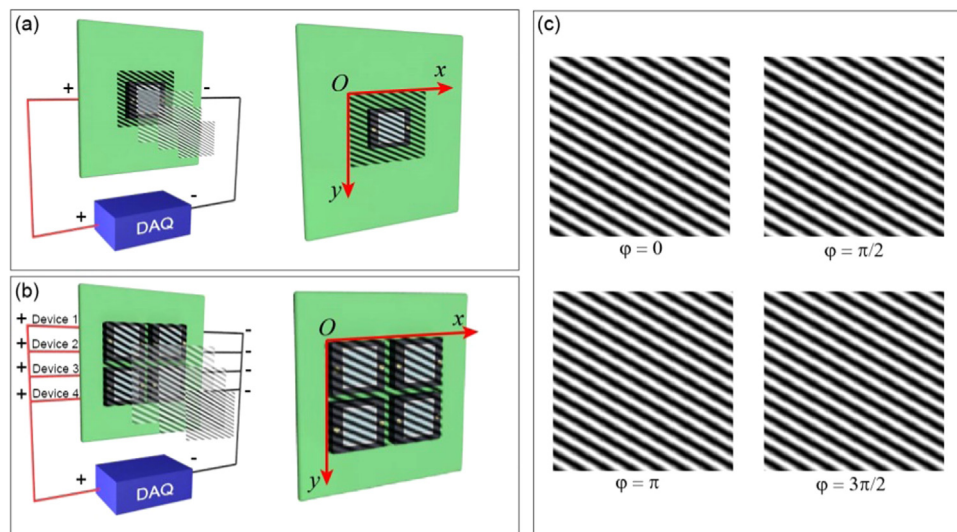
Fig. 1. Functional imaging by using Fourier basis patterns illumination. (a) Imaging of a single photovoltaic device, (b) imaging of a 2 × 2 photovoltaic devices array where the devices are configured in parallel, and (c) a set of 4-step phase-shifting Fourier basis patterns. DAQ refers to data acquisition board.

3. Results

The experimental set-up is shown in Fig. 2. We use a solar cell (HAMAMATSU S12915-1010BR) as the target photovoltaic device. We perform func-structural imaging to this solar cell in this experiment. In order to generate uniform, high-contrast, and high-resolution structured patterns, we use a 5.5-in. cell phone display (LS055R1SX03 by SHARP, 1440 × 2560 pixels). The patterns are shown on the display sequentially and projected onto the active area of the solar cell through Lens 1 and the beam splitter. The pixel pitch of the display is 0.04725 mm × 0.04725 mm, which is smaller than that of desktop displays. The smaller pixel pitch enables higher resolution for spatial information acquisition. It is because the imaging principle of this technique is subject to active single-pixel imaging [16–26] where image resolution is determined by the spatial resolution of the illumination patterns. In order to acquire the structure image of the target solar cell, we use another solar cell as a side detector to collect the reflected light from the target solar cell through the beam splitter and Lens 2. Both solar cells are driven by a customized amplifier circuit and the resultant electrical signals are collected by a data acquisition board (National Instruments 6343 USB). It should be noted that the output signals from the target solar cell enables reconstructing the functionality image of the target solar cell while the signals from the side detector enables reconstructing the structure image of the target solar cell. We generate a complete set of 256 × 256-pixel Fourier basis patterns for illumination. In other words, the reconstructed images are in the size of 256 × 256 pixels.

The acquired Fourier spectra and the corresponding reconstructed functionality image and structure image are shown in Fig. 3. In this experiment, the Fourier spectra are fully sampled from 131,072 measurements, as shown in Fig. 3(a) and (c). The functionality image [Fig. 3(b)] and the structure image [Fig. 3(d)] are obtained by conducting an inverse 2-D Fourier transform to the spectra. To reveal the relationship between the functional features and structural features, we fuse the two images to be a pseudo-color image, termed 'func-structure image'. The red channel of the func-structure image is the intensity of the functionality image and the green channel of the func-structure image is the intensity of the structure image. Thus, the func-structure image is with a unique 2-D color bar. The func-structure image and its color bar are shown in Fig. 3(e). As illustrated by the color bar, for any area with high reflectance and high photovoltaic response, it appears orange-yellow in the func-structure image; for any area with high reflectance but low response, it appears green; for any area with low reflectance but high response, it appears red; for any area with low reflectance but low response, it appears black. In short, areas with different functional and structural features are characterized by different colors. We also render a 3-D distribution of the solar cell's photovoltaic response in Fig. 3(f). A photograph of the target solar cell taken by a cell phone is given in Fig. 3(g).

As the functionality image shows in Fig. 3(b), there is a rectangle area that is most sensitive to light. The response over the rectangle area is uniform and the average normalized response within this area is 0.9230. The size of this rectangle area is 173 × 173 pixels, which means the area is exactly square. By converting the discrete coordinate
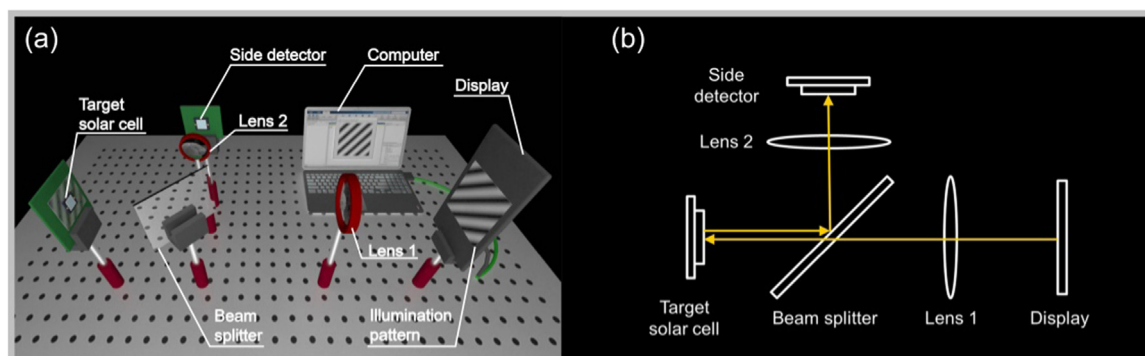

Fig. 2. Experimental set-up. (a) Schematic diagram of the set-up and (b) optical path.
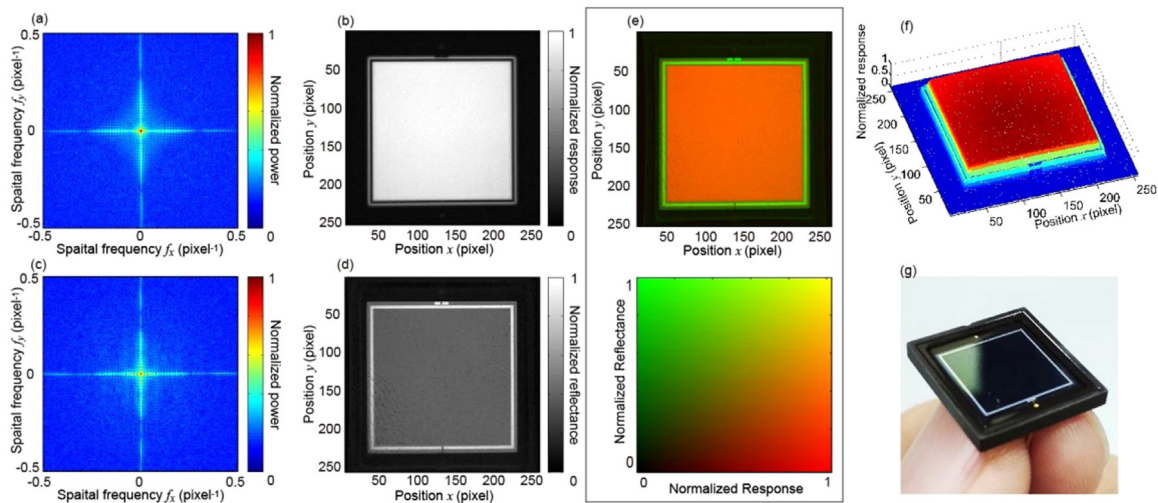
Fig. 3. Simultaneous functional and structural imaging result for a single solar cell. (a) Fourier spectrum of functionality image, (b) functionality image, (c) Fourier spectrum of structure image, (d) structure image, (e) fun-structure image and its 2-D color bar, and (f) 3-D reconstruction of the photovoltaic response distribution, and (g) photograph of the solar cell. (For interpretation of the references to color in this figure legend, the reader is referred to the web version of this article).

in the unit of pixel to the real physical coordinate in the unit of the millimeter, we find that the size of the area is $10 \times 10\,mm^2$, which coincides with the nominal value ($10 \times 10\,mm^2$) given in the manual of the product [27].

We surprisingly find that the solar cell has response outside the central active area. Such an area is in the shape of a narrow square ring and its normalized response on average is about 0.3921. The width of the narrow square ring is ∼ 3 pixels equivalent to 0.1734 mm. We also find that the outer response area is characterized by the indentation located at $y = {\sim}32$ and $x \in$(119, 139). Such an indentation can be clearly identified on the surface of the solar cell (see Fig. 3(g)). The outer response area is not depicted in the manual of the solar cell. Thus, the actual active area is larger than $10 \times 10\,mm^2$. Moreover, there is a gap between the central active area and the outer response area. The response within the gap tends to zero and corresponds to the white square ring in Fig. 3(d) and (g), which is evident by that the gap appears green in the func-structure image and the green color in the func-structure image implies low response and high reflectance.

We further perform simultaneous functional and structural imaging for multiple solar cells. We substitute the target solar cell shown in Fig. 2 with 4 solar cells. The solar cells are configured into a 2×2 array and connected in parallel, as Fig. 1(b) shows. We note that all these 4 solar cells were purchased from an online secondhand market. The manufacturer of the solar cells is unknown. These solar cells appear to be identical, according to its appearance. Each solar cell has an active area of $10 \times 10\,mm^2$.

Fig. 4 shows the functionality, structure, and func-structure images reconstructed from different sampling ratios. Please note that sampling ratio is referred to the number of measurements to the number of image pixels ratio. As the structure images show, all 4 solar cells are structurally-complete and have no obvious defects. However, as the functionality images show, there are only 3 solar cells functioning normally. Actually, we have noticed such a fact as early as only 60 measurements (sampling ratio = 0.0458%) were taken. As shown in Fig. 4(b), the func-structure image, though is blurred, apparently shows that the solar cell at the top-right corner corresponds to a green area, indicating that the solar cell is not functioning normally. Remind that green in the func-structure images means high reflectance but low response. As the images shown in Fig. 4(b) are derived from a sampling ratio of only 0.0458%, it demonstrates that the proposed technique allows for rapid characterization for multiple photovoltaic devices.

What's more, Fig. 4(a) shows that the bottom-left solar cell has a defect near the center of its active area. As Fig. 4(c) shows, such a defect
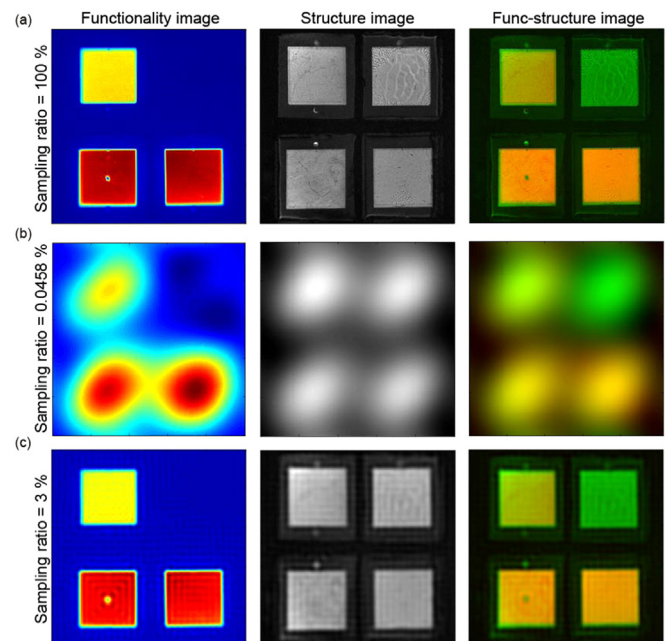

Fig. 4. Simultaneous functional and structural imaging result for a 2×2 solar cells array for different sampling ratios: (a) 100%, (b) 0. 0458%, and (c) 3%. The color bar for the func-structure images is the same as that shown in Fig. 3(e). (For interpretation of the references to color in this figure legend, the reader is referred to the web version of this article).

can be clearly identified even when the sampling ratio is about 3% (3932 measurements). The photovoltaic response at the suspected defect is significantly lower than elsewhere. This result further demonstrates that the proposed method enables rapid defects detection.

Moreover, we notice that the response of the top-left solar cell is globally weaker than that of the rest. It implies low effective quantum efficiency of the solar cell.

In order to investigate the cause of the defect, we capture an X-ray image of each solar cell using a Rayence 0505 A X-ray imager. It is believed that X-ray images can reveal the information about the inner structures of devices. As Fig. 5(a1) and (b1) show, both solar cells have a dark area around the center of their active area. We suspect the dark area is caused by some kind of metal used for welding the cathode of the solar cell. The metal strongly absorbs X-ray, which results in such a
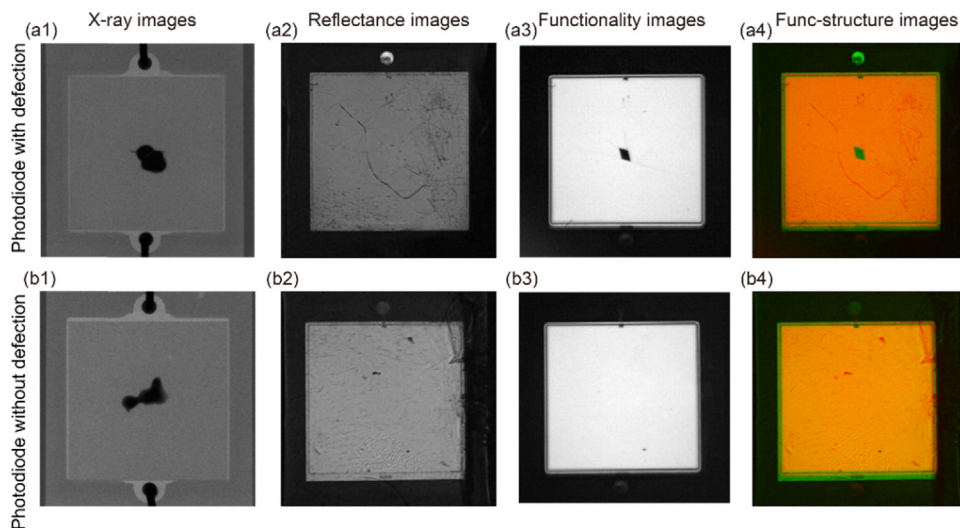
Fig. 5. Functionality images and structure (reflectance and X-ray) images of two second-hand solar cells. (a) solar cell without obvious abnormality and (b) solar cell with a suspected defect. The color bar for the func-structure images is the same as that shown in Fig. 3(e). (For interpretation of the references to color in this figure legend, the reader is referred to the web version of this article).

dark area. Remind that, neither the reflectance images nor the X-ray images show the functional difference between the two solar cells. Instead, the result by the proposed technique helps discover the defect. Please note that the field-of-view of the X-ray images shown in Fig. 5 is different from that of the images acquired with our experimental set-up. Thus, the X-ray images have to be cropped and finely registered to the images acquired with our experimental set-up. On the contrary, the reflectance and the functionality images acquired with our set-up are naturally registered and no image cropping or registration is required, which is one of the advantages of the technique.

Furthermore, we produce a few artificial defects on the target solar cell used in the first experiment by using a pulse laser. The solar cell with artificial defects is used for structural and functional imaging again. As the Fig. 6(a) shows, the artificial defects do not appear in the X-ray image. Instead, the artificial spots can be well identified in the structural image shown in Fig. 6(b). For the functional image shown in Fig. 6(c), there are also spots correspondingly, although the spots look blurred. The largest spot is pointed by the arrows. We consider that the laser only burnt the surface of the solar cell's active area, but not damaged the internal P-N junction. The spots on the surface of the active area are like an obstacle that prevents light from reaching the P-N junction. That is why we observe the blurred spots from the functionality image. The blurred spots are actually out-of-focus images of the spots on the active area surface. As the laser did not damage the inner structure of the solar cell, we can't find any defect in the X-ray image.

The series of experiments demonstrates that the proposed technique can achieve simultaneous functional imaging and structural imaging for a single and multiple photovoltaic devices. Additionally, func-structural imaging can be done with a relatively small number of measurements, which potentially enables characterization for photovoltaic device(s). The func-structure image provides rich information which allows manufacturers to improve their fabrication and users to monitor the 'health conditions' of the utilized devices.

4. Discussion

The imaging time is mainly limited by the structured light modulator. In our experiments, we use a cell phone LCD monitor to generate structured illumination. LCD monitors generally can switch illumination patterns at a rate of 120 Hz. However, the cell phone LCD monitor se utilize provides no hardware trigger. Thus, we have to use a software trigger and consequently the LCD operates at only 9 Hz. As a result, we spent ~ 4 h in taking 131,072 measurements the first experiment. Fortunately, the proposed technique, as demonstrated in the second experiment, enables imaging from undersampling data. We can successfully identify a failed solar cell with only 60 measurements (~ 7 s) and discover a suspected defect on a solar cell with 3932 measurements (~ 7 min). The reason why we use an LCD monitor for structured illumination is that the illumination generated by an LCD monitor is more uniform than that by using a DMD with a collimated light. The uniformity of illumination is of great significance, because non-uniformity in illumination will cause systematic error in functional image acquisition. We believe that using a DMD-based set-up can substantially accelerate the imaging process, but a finely collimated light source is required and the set-up will become more complicated. We also note that the proposed technique is computationally efficient. The image reconstruction process only takes a fast 2-D inversed Fourier transform which can be done within negligible times. On the contrast, compressive sensing based techniques commonly employ some iterative optimization algorithms and are therefore consume considerable computational times. Thus, the proposed technique has the advantage of computational efficiency.

Our experiments demonstrate the proposed technique allows for simultaneous functional and structural imaging for multiple solar cells. One can also perform simultaneous functional and structural imaging for a pixelated camera, such as a CCD camera and a CMOS camera. In this case, the imaging time will be determined by the shutter of the camera.
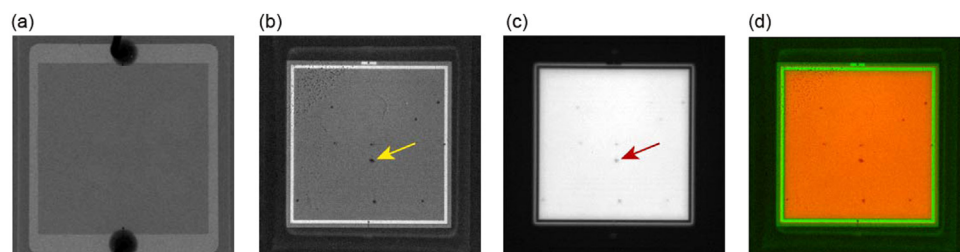

Fig. 6. Simultaneous functional and structural imaging result for a single solar cell with artificial defects. (a) X-ray image, (b) structure image, (c) functionality image, (e) func-structure image. The largest artificial burnt spot is pointed out by the arrows. The color bar for the func-structure image is the same as that shown in Fig. 3(e). (For interpretation of the references to color in this figure legend, the reader is referred to the web version of this article).

The proposed technique is potentially applicable for other photo-sensitive devices, such as photoacoustic, photochemical, or photo-thermal devices.

Moreover, semiconductor commonly exhibits the photoelectric effect. A semiconductor will absorb photos whose energy is greater than the bandgap and change behavior (such as, conductivity, luminescence, etc.). Thus, the proposed technique is also potentially applicable for screening defects inside some semiconductor-based die or 'chip'.

5. Conclusion

We propose an imaging simple, low-cost, effective, and efficient technique that can simultaneously acquire functionality and structure images of photovoltaic devices efficiently. As is experimentally demonstrated, the technique is able to simultaneously acquire functionality image and structure image of single or even 4 photovoltaic devices at the same time. The technique can also identify the failed device from 4 photovoltaic devices within ~ 7 s (sampling ratio = 0.0458%) and discover a suspected defect on a solar cell with ~ 7 min (sampling ratio = ~ 3%). The functional and structural information jointly provided by the technique allows not only users to monitor the 'health conditions' of the utilized devices, but also manufacturers to improve their fabrication. The proposed technique may find applications in rapid screening in semiconductor-based devices.

Competing interests

The authors declare no competing financial interests.

References

[1] J.H. Hafner, C.L. Cheung, A.T. Woolley, C.M. Lieber, Structural and functional imaging with carbon nanotube AFM probes, Prog. Biophys. Mol. Biol. 77 (2001) 73–110.
[2] X. Wang, Y. Pang, G. Ku, X. Xie, G. Stoica, L.V. Wang, Noninvasive laser-induced photoacoustic tomography for structural and functional in vivo imaging of the brain, Nat. Biotechnol. 21 (2003) 803.
[3] Y. Yang, A. Raine, Prefrontal structural and functional brain imaging findings in antisocial, violent, and psychopathic individuals: a meta-analysis, Psychiatr. Res. -Neuroimage 174 (2009) 81–88.
[4] K. Daniel, Z. Ninkov, Influence of non-uniform charge-coupled device pixel response on aperture photometry, Opt. Eng. 40 (2010) 162–170.
[5] P. Albert, Z. Ninkov, Subpixel sensitivity maps for a back-illuminated charge-coupled device and the effects of nonuniform response on measurement, Opt. Eng. 41 (2002) 1192–1203.
[6] J. Guo, R. Adato, D.J. Brady, Single-shot subpixel response measurement with an aperture array pixel mask, Opt. Lett. 31 (2006) 3441–3443.
[7] K. Daniel, Z. Ninkov, Subpixel sensitivity map for a charge-coupled device, Opt. Eng. 37 (1998) 948–955.
[8] N. Barron, M. Borysow, K. Beyerlein, M. Brown, W. Lorenzon, M. Schubnell, G. Tarlé, A. Tomasch, C. Weaverdyck, Subpixel response measurement of near-infrared detectors, Publ. Astron. Soc. Pac. 119 (2007) 466.
[9] P. Fumo, E. Waldron, J.P. Laine, G. Evans, Pixel response function experimental techniques and analysis of active pixel sensor star cameras, J. Astron. Telesc. Inst. 1 (2015) 028002.
[10] J. Hu, M. Song, Y. Sun, Y. Li, Measurement of modulation transfer function of charge-coupled devices using frequency-variable sine grating patterns, Opt. Eng. 38 (1999) 1200–1205.
[11] J.M. Flores-Moreno, M.H.D. la Torre-lbarra, M. del Socorro Herná[ndez-Montes, C.P. Lopez, F. Mendoza-Santoyo, CMOS and sCMOS imaging performance comparison by digital holographic interferometry, Opt. Eng. 55 (2016) 121728.
[12] M. Marchywka, D.G. Socker, Modulation transfer function measurement technique for small-pixel detectors, Appl. Opt. 31 (1992) 7198–7213.
[13] R. Gupta, O. Breitenstein, Digital micromirror device application for inline characterization of solar cells by tomographic light beam-induced current imaging, Proc. SPIE 6616 (2007) 66160O.
[14] S.R. Hall, M. Cashmore, J. Blackburn, G. Koutsourakis, R. Gottschalg, Compressive current response mapping of photovoltaic devices using MEMS mirror arrays, IEEE Trans. Instrum. 65 (2016) 1945–1950.
[15] G. Koutsourakis, M. Cashmore, S.R. Hall, M. Bliss, T.R. Betts, R. Gottschalg, Compressed sensing current mapping spatial characterization of photovoltaic devices, IEEE J. Photovolt. 7 (2017) 486–492.
[16] Z. Zhang, X. Ma, J. Zhong, Single-pixel imaging by means of Fourier spectrum acquisition, Nat. Commun. 6 (2015) 6225.
[17] G.M. Gibson, B. Sun, M.P. Edgar, D.B. Phillips, N. Hempler, G.T. Maker, G.P.A. Malcolm, M.J. Padgett, Real-time imaging of methane gas leaks using a single-pixel camera, Opt. Express 25 (2017) 2998–3005.
[18] M. Sun, M.P. Edgar, G.M. Gibson, B. Sun, N. Radwell, R. Lamb, M.J. Padgett, Single-pixel three-dimensional imaging with time-based depth resolution, Nat. Commun. 7 (2016) 12010.
[19] L.M. León, P. Clemente, Y. Mori, V. Climent, J. Lancis, E. Tajahuerce, Single-pixel digital holography with phase-encoded illumination, Opt. Express 25 (2017) 4975–4984.
[20] S. Ota, R. Horisaki, Y. Kawamura, Y. Kawamura, M. Ugawa, I. Sato, K. Hashimoto, R. Kamesawa, K. Setoyama, S. Yamaguchi, K. Fujiu, H. Waki, H. Noji, Ghost cytometry, Science 360 (2018) 1246–1251.
[21] Z. Zhang, S. Jiao, M. Yao, X. Li, J. Zhong, Secured single-pixel broadcast imaging, Opt. Express 26 (2018) 14578–14591.
[22] Z. Zhang, S. Liu, J. Peng, M. Yao, G. Zheng, J. Zhong, Simultaneous spatial, spectral, and 3D compressive imaging via efficient Fourier single-pixel measurements, Optica 5 (2018) 315–319.
[23] L. Bian, J. Suo, Q. Dai, F. Chen, Experimental Comparison of Single-Pixel Imaging Algorithms, 35 JOSA A, 2018, pp. 78–87.
[24] M. Sun, L. Meng, T., M.P. Edgar, M.J. Padgett, N. Radwell, A Russian Dolls ordering of the Hadamard basis for compressive single-pixel imaging, Sci. Rep.-UK 7 (2017) 3464.
[25] B. Sun, M.P. Edgar, R. Bowman, L.E. Vittert, S. Welsh, A. Bowman, M.J. Padgett, 3D computational imaging with single-pixel detectors, Science 340 (2013) 844–847.
[26] Z. Zhang, X. Wang, G. Zheng, J. Zhong, Hadamard single-pixel imaging versus Fourier single-pixel imaging, Opt. Express 25 (2017) 19619–19639.
[27] ⟨https://www.hamamatsu.com/resources/pdf/ssd/s12915_series_kspd1086e.pdf⟩.